# Size and Concentration Effects on the Photoluminescence of $La_2O_2S:Eu^{3+}$ Nanocrystals

**Qilin Dai,[†] Hongwei Song,*[,‡] Meiyuan Wang,[†] Xue Bai,[‡] Biao Dong,[‡] Ruifei Qin,[†] Xuesong Qu,[†] and Hui Zhang[†]**

*Key Laboratory of Excited State Physics, Changchun Institute of Optics, Fine Mechanics and Physics, Chinese Academy of Sciences, and Graduate School of Chinese Academy of Sciences, 16 Eastern Nan-Hu Road, Changchun 130033, People's Republic of China and State Key Laboratory of Integral Optoelectronics, College of Electronic Science and Engineering, JiLin University, Changchun 130012, People's Republic of China*

*Received: September 19, 2008; Revised Manuscript Received: October 22, 2008*

The effects of size and europium concentration on photoluminescence properties of $La_2O_2S:Eu^{3+}$ nanocrystals (~20 nm) and the corresponding bulk were studied. The results indicate that in nanocrystals, the absorption edge largely shifted to blue in comparison to the bulk, which was mainly attributed to the variation of phonon-excitation relaxation. Two excitation bands were observed, located at ~250 and ~330 nm, respectively, corresponding to the charge transfer (CT) transitions of Eu−O and Eu−S. Relative to the CT transition of Eu−O, that of Eu−S increased greatly with europium concentration. The dependence of photoluminescence intensity on concentration showed that in the nanocrystals and the bulk, $Eu^{3+}$ ions had two different quenching mechanisms, respectively, the exchange interaction and electric dipole−dipole interaction.

## I. Introduction

Lanthanide (La−Lu) oxysulfides with high chemical stability and high thermal stability are known as wide-gap (4.6−4.8 eV) materials suitable for doping ion activation.[1] In addition, compared with the lanthanide oxides, oxysulfide is a more efficient phosphor with a broader excitation band. Therefore, the lanthanide oxysulfides become a very important family of inorganic materials that have high potential for applications in various fields, such as color television picture tubes,[2] radiographic imaging,[3] field emission displays,[4,5] and long-lasting phosphorescence.[6−8] Among them, $Eu^{3+}$ activated lanthanide oxysulfide has been extensively investigated because it is a very efficient red phosphor applied in television picture tubes.

Studies on the luminescent properties of nanosized phosphors are currently attracting interest; because it is significant not only for applications but also for the essential understanding of nanocrystals, such as confinement effect, surface effect, etc. Among them, rare earth doped nanophosphors have attracted particular attention.[9−16] It is expected that in the nanosized phosphors, the luminescent quantum yield as well as the resolution of display be considerably improved. In addition, some rare earth ions, such as $Eu^{3+}$, may act as common activators to detect local environments[17] due to their supersensitive *f*−*f* transitions. Until now, a great number of rare earth doped nanosized phosphors have been prepared and studied,[18−20] especially the role of crystal structures, crystal sizes, and concentrations on the luminescence in oxide have been extensively studied.[21−23] However, the reports on nanosized lanthanide oxysulfides are rather few. In the past few years, there appeared only a few papers regarding the preparation and photoluminescence properties of rare earth doped lanthanide oxysulfides nanocrystals. Jagannathan developed two methods to obtain the $Y_2O_2S$ nanocrystals,[3,8] two step sol−gel polymer thermolysis method and gel-polymer thermolysis process; Zhigang Liu[24] synthesized the $La_2O_2S$ nanocrystals with a Gelatin-Template; and Hongshang Peng[25] reported a gel thermolysis method to prepare $La_2O_2S$ nanocrystals. Their results mainly concentrated onpreparation and characterization.[26,27] To completely understand the luminescent properties of lanthanide oxysulfides nanocrystals, comprehensive spectral and dynamic studies are required. In this work, the photoluminescence properties, especially the size and concentration effects of $La_2O_2S:Eu^{3+}$ nanocrystals were systematically studied.

## II. Experiments

**A. Sample Preparation.** The nanocrystals were prepared by combustion as reported by Jagannathan.[3] In a typical procedure, appropriate amounts high purity $La_2O_3$ and $Eu_2O_3$ powder was dissolved in hot concentrated $HNO_3$ to form $La(NO_3)_3$ $Eu(NO_3)_3$ solution, respectively. Then, $La(NO_3)_3$ and $Eu(NO_3)_3$ urea formaldehyde and sulfur were mixed together with a mol ratio of 2:0.002:5:3:3. The mixture was kept at 60 °C while stirring until it became a gel, and then the gel was ground into yellow powder. Next, the powders were annealed at 500 °C for 2 h. Finally, the white powders of $La_2O_2S:Eu^{3+}$ (0.1−40% mol) were obtained.

The bulk $La_2O_2S:Eu^{3+}$was prepared using a conventional solid state reaction method with the aid of sulfurizing flux. Stoichiometric amounts of $La_2O_3$, $Eu_2O_3$, S, and $Mg(OH)_2 \cdot 4MgCO_3 \cdot 6H_2O$ were mixed homogeneously blended with a flux of $Na_2CO_3$, S (S and $Na_2CO_3$ in a ratio of 1: 1 at 30 wt% of the total weight of raw material). The raw materials were sintered at 1150 °C for 2 h in a sealed crucible. The yellow powders were deal with hot dilute $HNO_3$ several times, then were heated at 80 °C and dried under vacuum for 2 h. Finally, the white powders of bulk $La_2O_2S:Eu^{3+}$ were obtained.

**B. Measurements.** X-ray diffraction (XRD) data were collected on a Rigaku D/max-rA X-ray diffractometer using a Cu

* To whom correspondence should be addressed. Fax: 86-431-85155129. E-Mail: hwsong2005@yahoo.com.cn.

† Key Laboratory of Excited State Physics, Changchun Institute of Optics, Fine Mechanics and Physics, Chinese Academy of Sciences, and Graduate School of Chinese Academy of Sciences.

‡ State Key Laboratory of Integral Optoelectronics, College of Electronic Science and Engineering, JiLin University.

10.1021/jp808343f CCC: $40.75 
Published on Web 11/16/2008

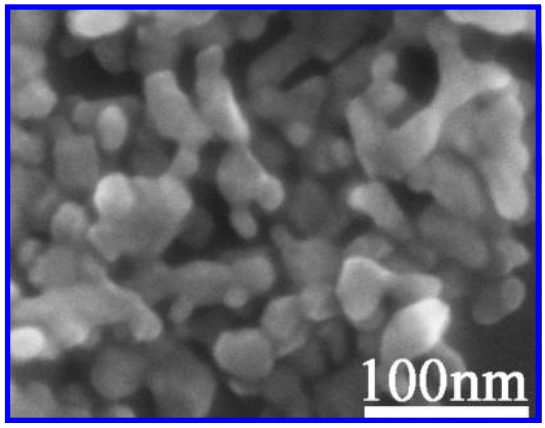


**Figure 1.** The SEM for the sample $La_2O_2S:Eu^{3+}$ nanocrystals (2% mol).

target radiation source. Field emission scanning electron microscopy (FE-SEM) was taken on a Hitachi S-4800 electron microscope. Fluorescence spectra and diffused reflectance spectra ($BaSO_4$ sample was used as a standard) were recorded at room temperature using a Hitachi F-4500 spectrophotometer equipped with a continuous 150W Xe-arc lamp. For comparison of different samples, the emission spectra were measured at a fixed bandpass of 0.2 nm with the same instrument parameters and 700 V for PMT voltage. In the experiments of spectral change induced by UV light-irradiation, the monochromic light separated from the same Xe-arc lamp was used as irradiation source, which was with a slit of 10 nm. In the measurements of high-resolution emission spectra and fluorescence dynamics, a 266-nm laser generated from a pulsed Nd:YAG (aluminum garnet) laser combined with a fourth-harmonic-generator was used as excitation. It was with a line width of 0.2 $cm^{-1}$, pulse duration of 10 ns and repetition frequency of 10 Hz. The experiment of frequency-selective excitation was performed at 77 K, in which the samples were put into a liquid nitrogen system. A Rhodamine 6 G dye pumped by the same Nd: YAG laser was used as the frequency-selective excitation source. A Spex 1403 spectrometer, a boxcar integrator were used to record the high-resolution emission spectra and dynamics.

## III. Results and Discussion

**A. Morphology and Crystalline Structure.** Figure 1 shows FE-SEM images of $La_2O_2S:Eu^{3+}$ nanocrystalline powders. It is obvious that all the powders yield nanoparticles and they tend to aggregate together. The average size of the nanoparticles is about 20 nm. Note that as the $Eu^{3+}$ concentration changed, the morphology and particle sizes almost did not change. Figure 2 shows the XRD patterns of different $La_2O_2S:Eu^{3+}$ powders in comparison to the standard card (JCPDS 27−0263). As seen, the crystal structure of all the samples belongs to the pure hexagonal phase. In comparison to the standard card, the XRD patterns of the nanopowders become broader, indicating the formation of nanocrystals. The diffraction peaks in the nanocrystals shift to the high angle side with the increasing doping concentration, implying that the $Eu^{3+}$ ions have been doped into the lattices of $La_2O_2S$. Because the radius of $Eu^{3+}$ is smaller than that of $La^{3+}$, the lattice constants become smaller while $Eu^{3+}$ substitutes $La^{3+}$. Estimated according to the Scherrer equation, the average crystalline size of the powders is determined to be 25 nm, which is basically in consistent with the crystalline size estimated by SEM images.

Figure 3 shows the diffused reflectance spectra of $La_2O_2S:Eu^{3+}$ in nanocrystals and bulk. The diffused spectra between

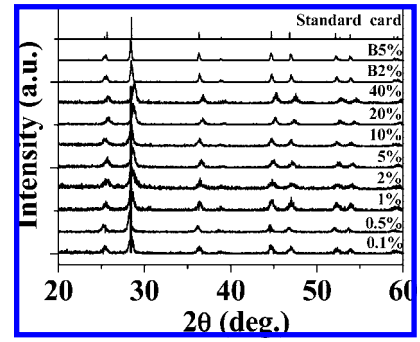


**Figure 2.** The XRD patterns for nanocrystals with different doping concentration and the bulk B2%: bulk doped with 2% $Eu^{3+}$; B5%: bulk doped with 5% $Eu^{3+}$.

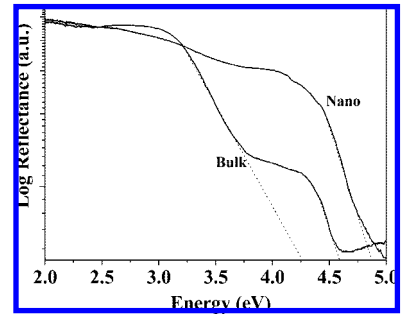


**Figure 3.** Diffused reflectance spectra of $La_2O_2S:Eu^{3+}$ for nanoparticles and bulk (2%).

the bulk and the nanocrystals show considerable difference. In the bulk, there exist two exponential steps, extending to 4.30 and 4.69 eV, respectively. The first step should correspond to the absorption edge of bulk $La_2O_2S$, which has a band gap of ~4.35 eV. As to the second step, its location is close to that in the nanocrystals. In the nanocrystals, there exists only one step, extending to 4.89 eV, which should correspond to the band edge of nanocrystalline $La_2O_2S$. This indicates that the absorption edge in the nanocrystals largely shifts to blue in comparison to that in the bulk. In the 20-nm $La_2O_2S$ nanocrystals, the size confinement effect could not induce such a large blue-shift of absorption edge. The present blue-shift in the $La_2O_2S$ nanocrystals can be mainly attributed to the increased exciton−phonon coupling in the nanocrystals. In $Y_2O_3:Eu^{3+}$ nanocrystals A. Konrad also[28] observed a blueshift of the absorption edge, depending on the particle size and temperature. It was suggested that the shift of the exciton energy resulted from an increase of the lattice relaxation energy $S_v\hbar\omega_v$ of the excited-state with decreasing particle size, which were attributed to the following two possible reasons. First, due to the surface of the nanocrystals a hydrostatic pressure caused by the Gibbs−Thomson effect might increase the phonon energy $\hbar\omega_v$ or the coupling constant $S_v$ due to the presence of strain. Second, the exciton phonon coupling constant may have particle size dependence, increasing with the decreased particle size, which has already been claimed for CdSSe nanocrystals.

**B. Dependence of Photoluminescence Spectra on $Eu^{3+}$ Concentration.** Figure 4, parts a and b, shows, respectively, the photoluminescnece spectra of $La_2O_2S:Eu^{3+}$ nanocrystals and bulk with different $Eu^{3+}$ concentrations. In the excitation spectra (left), there exist two excitation bands, locating around 250 and 330 nm, respectively, for both the nanoparticles and the bulk. The sharp line assigned to the $^7F_0-^5D_2$ transition of $Eu^{3+}$ at 467 nm can be also observed, especially for nanocrystals. As the doping concentration of europium is lower, the band peaking around 250 nm is dominant. Relative to the 250 nm

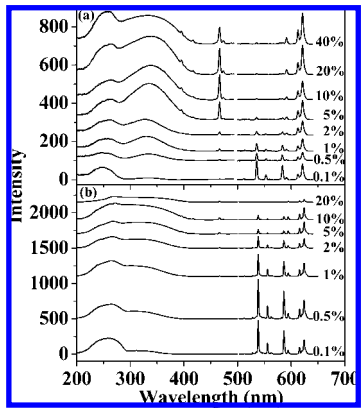


**Figure 4.** Excitation ($\lambda_{em} = 625$ nm) and emission spectra ($\lambda_{ex} = 250$ nm) of different samples (a) nanocrystals, (b) bulk.

band, the band peaking around 330 nm increases with the increasing europium concentration. The increase in nanocrystals is more obvious compared to that in the bulk. According to the literature,[24] the 250 nm and the 330 nm peaks are attributed to the charge transfer transitions of $O^{2-} \rightarrow Eu^{3+}$ and $S^{2-} \rightarrow Eu^{3+}$, respectively. In $La_2O_2S$, the $Eu^{3+}$ impurities will replace $La^{3+}$ ions, be coordinated to three sulfur and four oxygen ions and have $C_{3V}$ site symmetry. The interatomic distances are as follows: La−S, 3.07 A; La−O, 2.38 A; La−O′, 2.41 A. Therefore, it is not difficult to understand that the probability for the $O^{2-} \rightarrow Eu^{3+}$ charge transfer transition is larger than that for the $S^{2-} \rightarrow Eu^{3+}$ one. In both, the bulk and nanocrystals, some defect states are inevitably involved. As the $Eu^{3+}$ concentration increases, more $Eu^{3+}$ ions locate nearby the defect states, which can capture the excitation energy and quench the charge transfer transitions of $O^{2-} \rightarrow Eu^{3+}$ and $S^{2-} \rightarrow Eu^{3+}$. It is suggested that the quenching of defect states to the $O^{2-} \rightarrow Eu^{3+}$ charge transfer transition is greater than that to the $S^{2-} \rightarrow Eu^{3+}$ one.

In the emission spectra (right), transitions from the excited $^5D_J$ ($J = 0, 1$) to $^7F_J$ ($J = 1, 2$) levels of $Eu^{3+}$ ions are identified. The emission lines at 538, 556, and 587 nm originate from $^5D_1-^7F_J$ ($J = 1$, 2, and 3) transitions, respectively, while the lines peaking at 625 and 615 nm arise from the forced electric-dipole transitions of $^5D_0-^7F_2$. It can be seen that the intensity of $^5D_1-^7F_J$ gradually decreases with the increase of europium concentration, while that of the $^5D_0-^7F_2$ transitions gradually increases, for both the nanocrystals and the bulk, which is related to cross relaxation processes among $Eu^{3+}$ ions.

A comparison of the dependence of the $^5D_0-^7F_J$ or $^5D_1-^7F_J$ emission intensity on europium concentration between nanocrystals and bulk are shown in figure 5. In Figure 5a, it can be seen that under 330 nm excitation ($S^{2-} \rightarrow Eu^{3+}$) the intensity of $^5D_1-^7F_J$ increases as the $Eu^{3+}$ arises to 1% and then quenches quickly when the $Eu^{3+}$ increases sequentially, in both nanocrystals and bulk. As for the intensity of $^5D_0-^7F_J$, shown in Figure 5b, there exists an intensity maximum at 10% for the bulk, while exists a maximum at 20% for the nanocrystals under the same excitation, implying that the $^5D_0-^7F_J$ transition in nanocrystals has a larger quenching concentration over the bulk. Figure 5c shows that under the excitation of 250 nm ($O^{2-} \rightarrow Eu^{3+}$) the intensity of $^5D_1-^7F_J$ decreases gradually, for both the nanocrystals and the bulk. However, under the same excitation the intensity variation of $^5D_0-^7F_J$ in the two samples is very different. The intensity of $^5D_0-^7F_J$ increases with the increasing $Eu^{3+}$ concentration in the nanocrystals, on the contrary, it decreases with $Eu^{3+}$ concentration in the bulk, as shown in Figure 5d. The above results indicate that the $^5D_0$ level in nanocrystals has a larger quenching concentration in comparison to the bulk. This phenomenon was also observed in the other nanocrystals, such as nanocrystalline $Y_2O_3:Eu^{3+}$ and $YBO_3:Eu^{3+}$. It was suggested that in nanocrystals, the energy transfer from rare earth ions to inner defect states was hindered due to the boundary confinement of nanoparticles.[29,30]

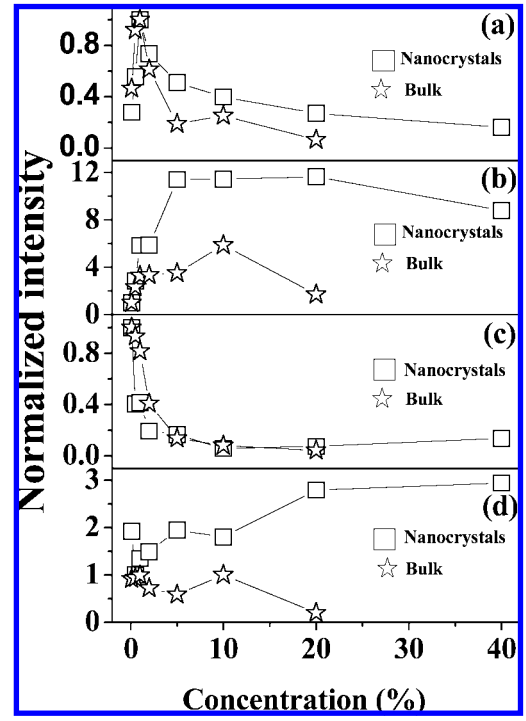


**Figure 5.** Dependence of emission intensity on $Eu^{3+}$ concentration measured at different wavelengths (a) $\lambda_{ex} = 330$ nm, $\lambda_{em} = 538$ nm ($^5D_1-^7F_1$); (b) $\lambda_{ex} = 330$ nm, $\lambda_{em} = 625$ nm ($^5D_0-^7F_2$); (c) $\lambda_{ex} = 250$ nm, $\lambda_{em} = 538$ nm; (d) $\lambda_{ex} = 250$ nm, $\lambda_{em} = 625$ nm.

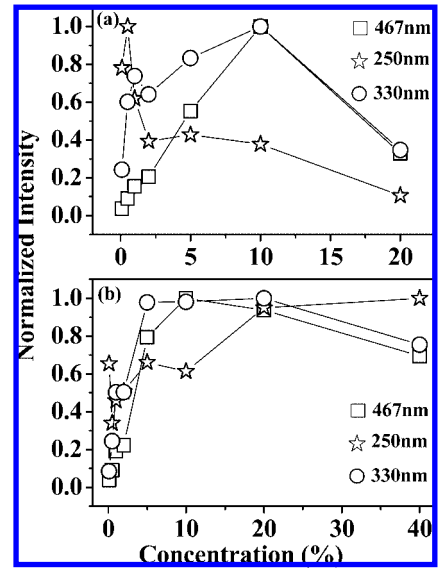


**Figure 6.** Dependence of $^5D_0-^7F_J$ emission intensity on $Eu^{3+}$ concentration under the excitaion of 467, 250, and 330 nm (a) In the bulk, (b) In the nanocrystals.

Figure 6 shows the emission intensity of $^5D_0-^7F_J$ as a function of europium concentration under the CT and $^7F_0-^5D_2$ direct excitation (at 467 nm). It can be seen that under the CT excitation at 330 nm and $^7F_0-^5D_2$ direct excitation, the emission intensity has a similar trend as a function of $Eu^{3+}$ concentration.

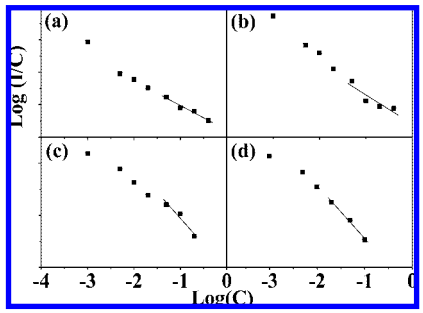


**Figure 7.** The relation between the concentration of $Eu^{3+}$ (C) and the log($I/C$). (a) $^5D_0 \rightarrow {}^7F_2$(nanocrystals), (b) $^5D_1 \rightarrow {}^7F_2$ (nanocrystals), (c) $^5D_0 \rightarrow {}^7F_2$ (bulk), and (d) $^5D_1 \rightarrow {}^7F_2$ bulk.

This indicates that under the 467 nm excitation, the $Eu^{3+}$ions corresponding to $S^{2-}$—$Eu^{3+}$ transitions have larger excitation or emission efficiency in comparison to those corresponding to $O^{2-}$—$Eu^{3+}$.

**C. Energy Transfer Type.** Huang[31] has previously developed a theoretical description on the relationship between the luminescent intensity and the doping concentration. Recent experimental results by Ou-Yang,[32] Li,[30] and Meng[33,34] have shown an agreement with the theoretical description. According to the Huang's result, the relationship between the luminescent intensity, $I$, and the doping concentration, $C$, can be expressed as follows:

$$I \propto \alpha^{(1-s/d)}\Gamma(1+s/d) \tag{1}$$

and

$$\alpha = C \bullet \Gamma(1-s/d)[X_0(1+A)/\gamma]^{d/s} \tag{2}$$

where $\gamma$ is the intrinsic transition probability of sensitizer, and $s$ is the index of electric multipole. The variable $d$ is the dimension of the sample, which would equal 3 since the energy transfer between $Eu^{3+}$ ions inside the particles is considered. $A$ and $X_0$ are constants. $\Gamma(1 + s/d)$ is a $\Gamma$ function. The values of $s$ are respectively, 6, 8, and 10 for the electric dipole−dipole, electric dipole−quadrupole and electric quadrupole−quadrupole interactions. The variable $s = 3$ corresponds to the mechanism of exchange interaction. From eqs 1 and 2, it can be derived that,

$$\log\left(\frac{I}{C}\right) = -\frac{s}{d}\log C + \log f \tag{3}$$

where $f$ is independent of the doping concentration.

Figure 7 shows the log($I/C$) − log($C$) plots for the $^5D_0$−$^7F_J$ and $^5D_1$−$^7F_J$ transitions of $Eu^{3+}$ in the nanocrystals and bulk. According to eq 3, using linear fittings to deal with the experimental data in region of high concentrations, the values of the slope parameter $-s/d$ were obtained, to be −0.8 and −1.1(close to 1), respectively, for the $^5D_0 \rightarrow {}^7F_J$ and $^5D_1 \rightarrow {}^7F_J$ transitions in the nanocrystals, corresponding to $s = 3$. This means that in the nanocrystals, the exchange interaction mechanism is dominant for the energy transfer among $Eu^{3+}$ ions. The slope parameters corresponding to the $^5D_0 \rightarrow {}^7F_J$ and $^5D_1 \rightarrow {}^7F_J$ transition in the bulk were deduced to be −2.0 and −2.01, which implies that the energy transfer is of electric dipole−dipole interaction type. It is well-known that different energy transfer types will show different distance dependencies. The effective distance of electric dipole−dipole interaction is much longer than that of exchange interaction. It is suggested that in the nanoparticles, the long-distance interaction was hindered to some content due to the existent of boundary of one nanoparticle.

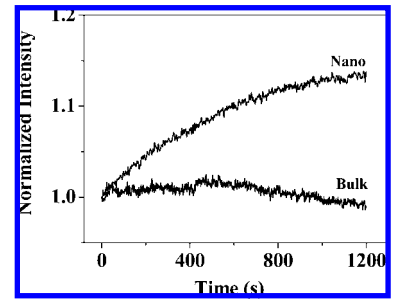


**Figure 8.** Dependence of emission intensity at 625 nm on irradiation time for nanocrystal and bulk (2% mol) ($\lambda_{ex} = 250$ nm).

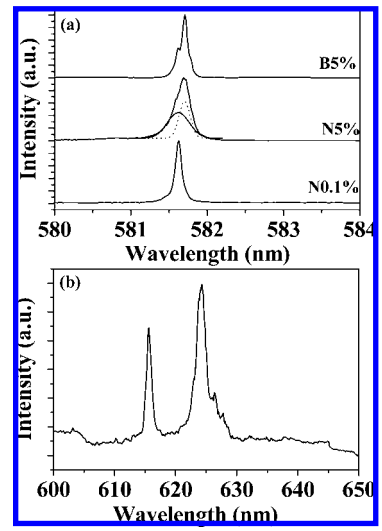


**Figure 9.** (a) $^7F_0$−$^5D_0$ excitation spectra monitoring $^5D_0$−$^7F_2$ emisson ($\lambda_{em} = 625$ nm) at 77 K. (b)$^5D_0$−$^7F_2$ emission spectrum under 581.52 nm excitation in sample N0.1%.

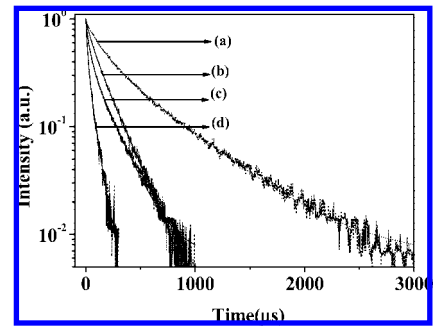


**Figure 10.** Fluorescence decay curves in the nanocrystals with different europium concentration, (a) Eu0.1%, $\lambda_{em} = 625$ nm, (b) Eu0.1%, $\lambda_{em} = 538$ nm (c) Eu40% $\lambda_{em} = 625$ nm (d) Eu40% $\lambda_{em} = 538$ nm. The scattered dots were experimental data and solid lines were fitting curves.

**D. UV-Light Irradiation Induced Intensity Enhancement.** The dependence of emission intensity of $Eu^{3+}$ on irradiation time under 280 nm excitation was measured and compared in nanocrystals and bulk (2 mol%), as shown in Figure 8. Ultraviolet light-irradiation induced intensity change is a universal phenomenon in nanocrystalline particles, which was first observed in ZnS:$Mn^{2+}$ nanocrystals and studied intensively in semiconductor nanoparticles.[35,36] The light-irradiation induced spectral change in $Y_2O_3$:$Eu^{3+}$ [14] and $Y_2O_3$:$Tb^{3+}$ [36]nanomaterials were systemically studied. It was observed that the luminescent intensity of $Y_2O_3$:$Eu^{3+}$ nanocrystals decreased, while that increased in $Y_2O_3$:$Tb^{3+}$ nanocrystals under UV-light irradiation. Presently, the luminescence intensity was enhanced

**TABLE 1: A List of Lifetime Constants, $\tau_1$ (shorter) and $\tau_2$ (faster) and Their Relative Contributions $R_1$ and $R_2$, Measured in Different Samples and Wavelengths**

| samples (concentration) | $\lambda_{em} = 538$ nm | | | | $\lambda_{em} = 625$ nm | | | |
|---|---|---|---|---|---|---|---|---|
| | $\tau_1(\mu s)$ | $R_1$ | $\tau_2(\mu s)$ | $R2$ | $\tau_1$ ($\mu s$) | $R_1$ | $\tau_2(\mu s)$ | $R_2$ |
| N0.1 | 70.6 | 0.514 | 213.2 | 0.486 | 154.7 | 0.613 | 624.3 | 0.387 |
| N0.5 | 44.2 | 0.648 | 159.2 | 0.352 | 69.34 | 0.667 | 377.8 | 0.333 |
| N1 | 43.8 | 0.676 | 150.7 | 0.324 | 68.9 | 0.659 | 415.3 | 0.341 |
| N2 | 21.6 | 0.691 | 108.8 | 0.309 | 114.8 | 0.609 | 598.5 | 0.391 |
| N5 | 22.8 | 0.762 | 91.6 | 0.258 | 140.9 | 0.629 | 561.5 | 0.371 |
| N10 | 15.7 | 0.820 | 64.6 | 0.180 | 60.3 | 0.629 | 353.4 | 0.371 |
| N20 | 24.8 | 0.920 | 114.2 | 0.080 | 41.0 | 0.72 | 245.3 | 0.28 |
| N40 | 18.7 | 0.904 | 92.6 | 0.096 | 29.3 | 0.792 | 197.6 | 0.208 |
| B0.1 | 28.3 | 0.096 | 160.6 | 0.904 | 168.3 | 0.346 | 341.4 | 0.654 |
| B0.5 | 35.6 | 0.130 | 159.0 | 0.870 | 147.4 | 0.125 | 326.7 | 0.875 |
| B1 | 28.7 | 0.157 | 151.4 | 0.843 | 138.1 | 0.059 | 326.6 | 0.941 |
| B2 | 30.8 | 0.271 | 140.0 | 0.723 | 124.6 | 0.24 | 317.3 | 0.76 |
| B5 | 29.1 | 0.530 | 116.0 | 0.470 | 72.6 | 0.27 | 301.4 | 0.73 |
| B10 | 20.5 | 0.726 | 112.6 | 0.274 | 62.4 | 0.267 | 298.6 | 0.733 |
| B20 | 14.3 | 0.861 | 98.1 | 0.139 | 32.0 | 0.567 | 346.0 | 0.433 |

under UV-light irradiation In $La_2O_2S:Eu^{3+}$ nanocrystals. It is suggested that during this process, the surface defects such as oxygen vacancies are modified, leading to the enhancement of photoluminescence. Note that the light-irradiation experiments were also performed under the excitation of 330 nm light, which demonstrated the same fact.

**E. Site Symmetry.** Figure 9a shows the $^7F_0-^5D_0$ excitation spectra monitoring $^5D_0-^7F_2$ site at 77 K. It can be seen that there exists one peak at 581.52 nm in nanocrystals 0.1% $Eu^{3+}$. When the doping concentration increased to 5%, the peak became broader. In the nanocrystals and the bulk, inner defect states should inevitably be involved, as we have mensioned above. When the $Eu^{3+}$ concentration is low, defect states have little influence on the transitions of $Eu^{3+}$, because the distance between a $Eu^{3+}$ ion and a nearest defect state is very far. As the $Eu^{3+}$ concentration increases, some $Eu^{3+}$ ions locate near to the defect states and the transitions of them shift due to disordered local environments. Figure 9b shows the $^5D_0-^7F_2$ emission spectra ($\lambda_{ex} = 581.52$ nm) at 77 K in N0.1% sample. It can be seen that the intensity of the peak at 625nm is a little higher than that at 615 nm. In fact, the emission spectra for the above three samples under the excitation of $\lambda_{ex} = 581.52$ nm and $\lambda_{ex} = 581.7$ nm were all measured and they are nearly the same. This suggests that there exists only one symmetry site in the nanocrystals and bulk.

**F. Fluorescence Dynamics.** Fluorescence decay curves in the nanocrystals with different europium concentrations monitoring 625 and 538 nm are shown in Figure 10. As can be seen, both the emissions can be fitted by a biexponential function. There existed two components, a faster one and a slower one, corresponding to different local surroundings. Table 1 lists the lifetime constants and their relative contributions for all the samples. It can be seen that both the fast and the slow components decreased with the increasing concentration, and decreased with crystal size. The fast component corresponds to the surroundings with more defect states and the slow component corresponds to the surroundings with less defect states. The contribution of the shorter component gradually increased with the increasing $Eu^{3+}$ concentration, whereas that of the longer component decreased. Note that the contribution of the shorter component increased from ~50 to 100% in nanocrystals, while that varied from nearly 0 to 100% in bulk for the emission at 538 nm. The fast component in nanocrystals takes more contribution compared to that in the bulk, for both emissions at 538 and 625 nm, implying more defect levels have been involved. From Table 1, both of the two decay time constants decreased with the increasing doping concentration, which was attributed to increased nonradiative relaxation rates due to cross relaxation processes among $Eu^{3+}$ ions. In some europium doped oxide nanocrystals, it was observed that the luminescent lifetime decreased with the size decrease of nanoparticles, while in the other nanocrystals the lifetime increased with the size decrease.[37,38] The former fact was generally attributed to the increase of nonradiative transition rate caused by surface defects in nanocrystals, whereas the latter fact was usually attributed to decreased radiative transition rate induced by the variation of effective refractive index. The radiative transition rate can be derived as follows:[39]

$$\tau_R \approx \frac{1}{f(ED)} \frac{\lambda_0^2}{\left[\frac{1}{3}(n^2+2)\right]^2 n} \tag{4}$$

where $f$(ED) is the oscillator strength for the electronic dipole transition, $\lambda_0$ is the wavelength in vacuum, and $n$ is the refractive index of the material. R. S. Meltzer et al. observed that the radiative lifetime of the nanocrystals depended not only on the refractive index itself but also on the surrounding medium and deduced that in nanoparticles $n$ in eq 4 should be substituted by the effective index $n_{eff} = xn + (1 - x)n_{med}$, where $x$ is the filling factor showing what fraction of the space is occupied by the nanoparticles and $n_{med}$ is the refractive index of the surrounding media.[12], Here $n_{med}$ should be close to 1 because the lifetime measurement was performed in air, which is smaller than $n$, the refractive index of $La_2O_2S$. Owing to $n_{eff} < n$, the radiative lifetime in nanocrystals increases in comparison to the bulk.

## IV. Conclusions

We have studied the size and concentration effects of photoluminescnece in $La_2O_2S$ $Eu^{3+}$ nanocrystals and the corresponding bulk. The results demonstrate the following: (1) the doping concentration of $Eu^{3+}$ can change the relative intensity of $S^{2-}-Eu^{3+}$ to $O^{2-}-Eu^{3+}$ components in excitation spectra for nanocrystals rather than bulk. (2) In the nanocrystals, the exchange interaction is a dominant mehcanism for the energy transfer proceesses of $Eu^{3+}$, while in the bulk electric dipole−dipole interaction is dominant. (3) The photoluminescence in nanoparticles is enhanced under UV-light irradiation, because the surface defects in nanocrystals are modified during the irradiation. (4) The luminescence for both nanocrystals and bulk decay biexponentially under UV-light irradiation.

**Acknowledgment.** This work is supported by the National Nature Science Foundation of China (Grant Nos. 50772042, 10704073, and 10504030) and the 863 project of China (2007AA032314).

## References and Notes

(1) Pires, A.; Serra, O.; Davolos, M. *J. Alloy. Compd.* **2004**, *374*, 181.
(2) Royce, M.; Smith, A. *Electrochem. Soc. Extd. Abstr.* **1968**, *34*, 94.
(3) Dhanaraj, J.; Jagannathan, R.; Trivedi, D. *J. Mater. Chem.* **2003**, *13*, 1778.
(4) Cho, S.; Yoo, J.; Lee, J. *J. Electrochem. Soc.* **1998**, *145*, 1017.
(5) Yoo, J.; Lee, J. *J. Appl. Phys.* **1997**, *81*, 2910.
(6) Kang, C.; Liu, R. *Chem. Mater.* **2003**, *15*, 3966.
(7) Thirumalai, J.; Jagannthan, R.; Trivedi, D. *J. Lumin.* **2007**, *2*, 353.
(8) Dhanarj, J.; Geethalakshmi, M. *Chem. Phys. Lett.* **2004**, *387*, 23.
(9) Meyssamy, H.; Riwotzki, K. *Adv. Mater.* **1999**, *11*, 840.
(10) Yada, M.; Mihara, M.; Mouri, S. Kijima. *Adv. Mater.* **2002**, *14*, 309.
(11) Wang, X.; Li, Y. *J. Eur. Chem.* **2003**, *9*, 5627.
(12) Meltzer, R.; Feofilov, S.; Tissue, B. *Phys. Rev. B* **1999**, *60*, 14012.
(13) Williams, D.; Bihari, B.; Tissue, B.; McHale, J. *J. Phys. Chem. B* **1998**, *102*, 96.
(14) Song, H.; Chen, B.; Peng, H.; J.; Zhang, J. *Appl. Phys. Lett.* **2002**, *81*, 1776.
(15) Shin, J.; Hoven, G.; Polman, A. *Appl. Phys. Lett.* **1995**, *66*, 2379.
(16) Fu, M.; Yoshida, M.; Kanzawa, Y.; Hayashi, S.; Yamamoto, K. *Appl. Phys. Lett.* **1997**, *77*, 1198.
(17) Song, H.; Yu, L.; Lu, S.; Wang, T.; Liu, Z.; Yang, L. *Appl. Phys. Lett.* **2004**, *85*, 470.
(18) Yu, L.; Song, H.; Lu, S.; Liu, Z.; Yang, L. *Chem. Phys. Lett.* **2004**, *399*, 384.
(19) Wu, C.; Qin, W.; Qin, G.; Zhao, D.; Zhang, J.; Huang, S. *Appl. Phys. Lett.* **2003**, *82*, 520.
(20) Jia, C.; Sun, L.; Luo, F.; Jiang, X.; Wei, L.; Yan, C. *Appl. Phys. Lett.* **2004**, *84*, 5305.
(21) Maciel, S.; Patra, A. *J. Opt. Soc. Am. B* **2004**, *21*, 681.
(22) Patra, A. *Chem. Phys. Lett.* **2004**, *387*, 35.
(23) Saha, S.; Chowdhury, P. S.; Patra, A. *J. Phys. Chem. B* **2005**, *109*, 2699.
(24) Liu, Z.; Sun, X.; Xu, S.; Lian, J.; Li, X.; Xiu, Z.; Li, Q.; Huo, D.; Li, J. *J. Phys. Chem. C* **2008**, *112*, 2353.
(25) Peng, H.; Huang, S.; You, F.; Chang, J.; Lu, S.; Cao, L. *J. Phys. Chem. B* **2005**, *109*, 5774.
(26) Pires, A.; Serra, O.; Davolos, M. *J. Alloy. Compd.* **2004**, *374*, 181.
(27) Zhao, F.; Gao, S. *J. Mater. Chem.* **2008**, *18*, 949.
(28) Konrad, A.; Herr, U.; Tidecks, R.; Kummer, F.; Samwer, K. *J. Appl. Phys.* **2001**, *90*, 3516.
(29) Wei, Z.; Sun, L.; Liao, C.; Yin, J.; Jiang, X.; Yan, C. *J. Phys. Chem. B* **2002**, *106*, 10610.
(30) Li, D.; Lu, S.; Zhang, J.; Liu, J.; Wang, H.; Sun, L.; Huang, S. *Chin. J. Lumin.* **2000**, *21*, 134.
(31) Huang, S.; Lou, L. *Chin. J. Lumin.* **1990**, *11*, 36.
(32) Ou-Yang, F.; Tang, B. *Rare Metal Mater. Eng.* **2003**, *32*, 522.
(33) Li, D.; Lu, S.; Wang, H.; Chen, B.; Zhang, J.; Huang, S. *Chin. J. Lumin.* **2001**, *22*, 227.
(34) Meng, Q.; Chen, B.; Xu, W.; Yang, Y.; Zhao, X.; Di, W.; Lu, S.; Wang, X. *J. Appl. Phys.* **2007**, *102*, 093505.
(35) Jin, C.; Yu, J.; Sun, L.; Dou, K.; Zhao, J.; Zhou, F.; Chen, Y.; Huang, S. *J. Lumin.* **1996**, *315*, 66.
(36) Wang, J.; Song, H.; Sun, B.; Ren, X.; Chen, B.; Xu, W. *Chem. Phys. Lett.* **2003**, *379*, 507.
(37) Peng, H.; Song, H.; Chen, B.; Wang, J.; Lu, S.; Kong, X. *J. Chem. Phys.* **2003**, *118*, 3277.
(38) Williams, D.; Yuang, H.; Tissue, B. *J. Lumin.* **1999**, *297*, 83.
(39) Henderson, B.; Imbusch, G. *Optical Spectroscopy of Inorganic Solids*; Clarendon Press: Oxford, 1989; p 173.

JP808343F